Journal of Intelligent & Robotic Systems (2022) 106: 4
https://doi.org/10.1007/s10846-022-01691-4

SHORT PAPER

L1 Adaptive Structure-Based Nonlinear Dynamic Inversion Control for Aircraft with Center of Gravity Variations

Yu Li[1] · Xiaoxiong Liu[1] · Qizhi He[1] · Ruichen Ming[1] · Wei Huang[1] · Weiguo Zhang[1]

Received: 1 June 2021 / Accepted: 8 July 2022 / Published online: 18 August 2022

Abstract
Due to the reliance on model knowledge and the lack of compensation mechanism, Nonlinear Dynamic Inversion (NDI) control does not provide the essential robustness in the face of disturbances such as the Center of Gravity (CG) sudden change. To overcome this deficiency, a novel adaptive NDI control approach based on the L1 adaptive structure, called L1 Adaptive Nonlinear Dynamic Inversion (L1-ANDI), is presented, which can guarantee the desired dynamic performance while overcoming the influence of disturbances and uncertainties. In particular, the introduction of a low-pass filter makes the L1-ANDI control realize the decoupling of fast adaptation and robustness. Furthermore, the effect of CG variations on the aircraft is analyzed from the aerodynamic perspective, and the L1-ANDI-based flight controller is designed to eliminate the influence of the CG variations. A series of simulation results demonstrate that the designed flight controller can achieve satisfactory performance and is robust to the disturbance of CG sudden variations.

Keywords Nonlinear Dynamic Inversion · L1 Adaptive control · Low-Pass Filter · Flight Control System · The Center of Gravity Variations

1 Introduction

The Center of Gravity (CG), one of the critical parameters for the aircraft, is directly related to stability and handing quality. The CG variations may cause the aircraft to deviate from its normal dynamics, or worse, it may destroy the original stability, which is a serious threat to safe flight. Therefore, it is of great significance to improve the robustness of the flight control law for aircraft with CG variations.

From the aerodynamics point of view, the inherent characteristics of the CG make its variations inevitably bring additional moments, further resulting in cross-coupling between the pitch, roll, and yaw channels. Its complexity determines that the traditional gain-scheduling approaches are difficult to cope with this challenge, that is, to overcome disturbances caused by the CG variations while ensuring the desired dynamic performance of the aircraft after the CG variations. Nevertheless, the maturity of nonlinear control methods presents a promising solution.

Nonlinear Dynamic Inversion (NDI), as a widely used feedback linearization nonlinear control technical, eliminates the nonlinearities in the system and the coupling between the channels through a feedback inversion strategy, thus ensuring the desired dynamics of the system. Because it does not require a tedious and complicated gain-scheduling and has the advantages of rapidity and strong decoupling ability, the NDI technical has been widely applied in the control law design of VSTOL aircraft [1, 2], fighters [3, 4], hypersonic vehicle [5], etc. Due to its reliance on accurate model knowledge, the NDI control exposes the problem of insufficient robustness in the face of model uncertainties and disturbances. Sieberling S and Wang X adopted the Incremental NDI (INDI) approach to enhance the robustness of a flight control system [6, 7]. However, as a significant feedback signal, the accuracy of angular acceleration signals is directly related to the robustness of the INDI control. To the best of the author's knowledge, angular acceleration signals are usually obtained by way of numeric differentiation of filtered angular rates. In this process, differentiation and filtering inevitably reduce the accuracy and real-time performance of angular accelerations, thereby deteriorating the robustness of INDI control. Therefore, the practical problem of how to obtain

✉ Yu Li
li_yu@mail.nwpu.edu.cn

[1] Department of Automation, Northwestern Polytechnical University, Xi'an, Shannxi, China

accurate angular accelerations hinders the application of the INDI technique in practice.

Another way is to integrate an adaptive structure into the NDI control approach to improve its robustness, whose type of improvement is called Adaptive Dynamic Inversion (ANDI). This technology has been widely developed and applied in several fields [8–11]. I.M. Mehedi. et al. proposed an adaptive generalized NDI based on sliding mode control and applied it to angular position tracking of the rotary flexible joint system [8]. Qizhi He. et al. combined observer and NDI to propose an observer-based RNDI control for designing the fault-tolerant controller of damaged aircraft [9]. L. Wang employed the ANDI to design the automatic carrier landing control law to reject the disturbance of the air wake and lateral coupling [10]. Joshi, Girish and Radhakant Padhi incorporate neural network technology in NDI control and propose a robust nonlinear control, which is successfully solved the challenging problem of satellite formation flying [11].

In the adaptive control structure, the adaptive algorithm acts as a compensation mechanism to estimate the impact of uncertainties and disturbances based on dynamic errors. Further, the controller compensates the system based on the estimated results. Therefore, adding an adaptive structure to NDI control is a reasonable and effective way to enhance the robustness of the system subjects to disturbances and uncertainties.

L1 adaptive control, an adaptive control approach with excellent performance and strong robustness, was first proposed by Cao C and Naira Hovakimyan in the 2006 American control conference [12]. This adaptive approach developed from the Model Reference Adaptive Control (MRAC). By adding a low-pass filter, the L1 adaptive controller solves the problem in the traditional MRAC that excessive adaptive gain tends to cause oscillations. In addition, the L1 adaptive control not only makes the system robust to model uncertainties and disturbances but also realizes the decoupling of robustness and fast adaptation. Therefore, the L1 adaptive control technical has received great attention after it was proposed, and it has been successfully applied in many aspects [13–21]. Heusden K V proved the L1 adaptive feedback control approximates an implementable LTI controller and explained why L1 adaptive control does not require sufficiency of excitation [22]. Divine Maalouf applied L1 adaptive control to underwater vehicles and tested the closed-loop system performance in different experimental scenarios [23]. For the nonsquare MIMO system, Hanmin Lee developed an L1 adaptive controller for a missile longitudinal autopilot. Results demonstrated that the designed controller could improve the performance over the stand-alone autopilot and achieve the desired performance [24]. Tyler Leman applied the L1 adaptive control to an X-48B aircraft flight control law. The effectiveness of the controller has been verified at different state points. Even in the case of severe cross-coupling and control surface failures, the L1 adaptive-based controller ensured uniform transient and steady-state performance in the whole flight envelope [25]. From the above research results, the L1 adaptive control technique can effectively overcome the influence of disturbances and is expert in solving the control problem of the complex system, including uncertainties and unmolded dynamics.

To enhance the robustness of NDI control, the L1 adaptive structure, as a compensation mechanism, is introduced into the NDI control. So a novel L1 Adaptive Nonlinear Dynamic Inversion (L1-ANDI) control approach is proposed in this paper, which not only retains the fast decoupling of NDI, but also inherits excellent robustness and fast adaptation of L1 adaptive control. Further, the proposed L1-ANDI control structure is applied to nonlinear aircraft to address the problem of the CG variations. Moreover, the nonlinear aircraft model with CG variations is established, and the influence caused by the CG shift is also analyzed.

The rest of this paper is organized as follows. Section 2 analyzes the NDI control system and formulates the control problem. The L1-ANDI control technique is presented, and its stability is analyzed in Section 3. In Section 4, the aircraft model with CG variations is established, and the flight control law is designed based on the proposed L1-ANDI method. In Section 5, the designed flight controller is simulated and verified under the disturbance of the CG sudden shifts. Finally, Section 6 concludes this paper.

2 Nonlinear Dynamic Inversion

As a typical nonlinear control method, NDI utilizes a strategy of feedback inversion to eliminate the nonlinear terms of the system, thus guaranteeing the system to achieve the desired dynamic behavior.

Generally, the nonlinear system can be described as:

$$\begin{cases} \dot{x}(t) = f(x) + G(x)\lambda\, u(t) + \xi(x,t) \\ y(t) = Cx(t) \end{cases} \tag{1}$$

where, $x(t)\in\mathbb{R}^n$, $u(t)\in\mathbb{R}^m$, and $y(t)\in\mathbb{R}^m$ are the system states, control inputs, and outputs, respectively. $f(x)\in\mathbb{R}^n$represents the nonlinear matrix of system the independent of control, and $G(x)\in\mathbb{R}^{n\times m}$ represents the nonlinear control matrix. $\lambda\in\mathbb{R}^{m\times m}$is the control effectiveness matrix with known symbols, $C\in\mathbb{R}^{m\times n}$is the output distribution matrix. $\xi(x,t)\in\mathbb{R}^n$denotes unknown nonlinear interferences, including external disturbances, parameter uncertainties, and unmodeled dynamics.

The system (1) can be reasonably rewritten as

$$\begin{cases} \dot{x}(t) = f(x) + G(x)(\lambda\, u(t) + \delta(x,t)) \\ y(t) = Cx(t) \end{cases} \tag{2}$$

with

$$\xi(x,t) = G(x,t)\delta(x,t) \tag{3}$$

The system satisfies the following assumptions:

Remark 1 Taking the aircraft as a background, it is reasonable to assume that the nonlinear system order n is equal to the number of input order m, that is, $n=m$. Additionally, the outputs coincide typically with the control states and are assumed to be physically similar. For example, three angular rates or attitude angles. For the system whose order n is greater than the number m of inputs ($n>m$), the singular perturbation theory can be employed to separate the states on time scales, that is, the states can be cascade controlled according to the speed of the response. On the contrary, for the system with $n<m$, a generalized NDI approach can be applied, as detailed in Refs [26, 27].

Assumption 1 Disturbance $\delta(x,t)$ is globally bounded. There exist positive constants D and X, and the $\delta(x,t)$ is bounded hold all $t>0$ provided that the states are bounded $\|x(t)\|_\infty \le X$.

$$\|\delta(x,t)\|_\infty \le D$$

Assumption 2 There are $d_{\delta,x}>0$ and $d_{\delta,t}>0$, the partial derivatives of the $\delta(x,t)$ are semi-global uniformly bounded.

$$\left\|\frac{\partial \delta(x,t)}{\partial x}\right\|_\infty \le d_{\delta,x}, \left\|\frac{\partial \delta(x,t)}{\partial t}\right\|_\infty \le d_{\delta t} \tag{4}$$

Assumption 3 Uniform boundedness of control effectiveness matrix.

$$\lambda \in \Lambda \triangleq [0,1] \tag{5}$$

Inspired by Ref [28], as long as the state $x(t)$ is differentiable or piecewise differentiable, the $\delta(x,t)$ can be further linearly parameterized.

$$\delta(x,t) = \vartheta(t)\|x(t)\|_\infty + \sigma(t) \tag{6}$$

Assumption 4 $\vartheta(t)$ and $\sigma(t)$ satisfy the following boundary conditions

$$\begin{aligned} &\|\vartheta(t)\|_\infty \le \vartheta_b, \quad \|\sigma(t)\|_\infty \le \sigma_b \\ &\|\dot{\vartheta}(t)\|_\infty \le d_\vartheta, \quad \|\dot{\sigma}(t)\|_\infty \le d_\sigma \end{aligned} \tag{7}$$

When there is no disturbance, and the system model is completely known, that is $\lambda = I_n$ and $\delta(x,t)=0$, the NDI control law is designed as:

$$u(t) = G(x)^{-1}\left(\nu_{des}(t) - f(x)\right) \tag{8}$$

where $\nu_{des}(t)$ is the virtual control that represents the expected dynamic behavior of the system. At this time, the system under NDI control law is $\dot{x}(t) = \nu_{des}(t)$. It means that the system response reaches the desired dynamic under ideal conditions.

If there are interferences such as external disturbances and model uncertainties, the dynamic of the system becomes

$$\dot{x}(t) = \nu_{des}(t) + \tau(x,t) \tag{9}$$

with

$$\tau(x,\ t) \triangleq G(x)\left(\vartheta(t)\|x(t)\|_\infty + \sigma(t) + \left(\lambda - I_n\right)u(t)\right) \tag{10}$$

Obviously, suffering from disturbances, the system response no longer satisfies the desired dynamics. It reveals that the NDI control lacks the essential robustness to disturbances, which hinders its application in practice. In terms of enhancing the robustness, combined with L1 adaptive structure, this paper proposes a robust ANDI control method called L1-ANDI.

3 L1 Adaptive Nonlinear Dynamic Inversion

As the name indicates, the L1-ANDI control is composed of NDI control and L1 adaptive structure. The former is still utilized to cancel the known nonlinear terms of the system, while the latter is implemented to overcome the effects caused by disturbances. In terms of the architecture, the L1 adaptive structure includes three parts, consisting of an adaptive law, a state predictor, and a controller with a low-pass filter.

3.1 Control law

L1-ANDI control law consists of two parts: NDI control $u_{NDI}(t)$ and L1 adaptive control $u_{L1}(t)$.

$$u(t) = u_{NDI}(t) + u_{L1}(t) \tag{11}$$

with

$$u_{NDI}(t) = \left(G(x)\hat{\lambda}(t)\right)^{-1}\left(\nu_{des}(t) - f(x)\right) \tag{12}$$

$$\begin{aligned} u_{L1}(s) &= -K_D D(s)\hat{\eta}(s) \\ \hat{\eta}(t) &\triangleq \hat{\lambda}(t)u_{L1}(t) + \hat{\vartheta}(t)\|x(t)\|_\infty + \hat{\sigma}(t) \end{aligned} \tag{13}$$

where s is the Laplace operator. The virtual control$\nu_{des}(t)$ is designed as

$$\nu_{des}(t) = A_m\left(x(t) - x_{cmd}(t)\right) \tag{14}$$

among them, $x_{cmd}(t)$ is the command signal, $A_m \in \mathbb{R}^{n\times n}$is the Hurwitz matrix, representing the expected dynamic characteristics of the system. Since the disturbances are unknown, the estimated values $\hat{\lambda}(t)$, $\hat{\vartheta}(t)$, and $\hat{\sigma}(t)$ generated by the adaptive law are used instead of $\lambda(t)$, $\vartheta(t)$, and $\sigma(t)$. The filter gain $K_D>0$ and the transfer function $D(s)$ are both filter components, and the specific form of the corresponding low-pass filter is:

$$C(s) = \frac{\lambda K_D D(s)}{1 + \lambda K_D D(s)}, C(0) = 1 \tag{15}$$

Remark 2 As key parameters, the choice of $D(s)$, K_D, and λ must satisfy the following L1-norm condition [12].

$$\left\| \left(sI - A_m\right)^{-1} G(x)(1 - C(s)) \right\|_{L1} \vartheta_b < 1 \tag{16}$$

To simplify the structure, let$D(s) = \frac{1}{s}$, and the low-pass filter becomes$C(s) = \frac{\lambda K_D}{s+\lambda K_D}$. Although the L1-norm condition (16) can always be satisfied by choosing a sufficiently large filter bandwidth λK_D, this may lead to a closed-loop system with overly small robustness margins, susceptible to measurement noise, and even oscillations. Therefore, the choice of bandwidth λK_D and $D(s)$ requires a combination of L1-norm condition and system robustness.

The low-pass filter plays two roles in the control law (13), as follows:

1. The introduction of a low-pass filter is sufficient to cancel out undesirable high-frequency dynamics of the parameters estimated by the adaptive law, which prevents the system from oscillations due to fast adaptation.

2. Since the controller (13) only compensates for the low-frequency part of disturbances, the existence of the low-pass filter is capable of allowing larger adaptation gain. It solves the problem of insufficient rapidity in the traditional adaptive structure due to low adaptation gain so that L1-ANDI control satisfies the robustness requirements while taking into account the rapid response of the system.

3.2 State predictor

Under the action of the control law, the state predictor has the desired dynamics of the system, which can be designed as follows

$$\begin{cases} \dot{\hat{x}}(t) = A_m \hat{x}(t) - A_m x_{cmd}(t) \\ \quad + G(x)\left(\hat{\lambda}(t) u_{L1}(t) + \hat{\vartheta}(t)\|x(t)\|_\infty + \hat{\sigma}(t)\right) \\ y(t) = C\hat{x}(t) \end{cases} \tag{17}$$

where $\hat{x}(t) \in \mathbb{R}^n$ represents the predictor state.

3.3 Adaptive law

According to errors between the system and the state predictor, the adaptive law updates the estimates of$\hat{\lambda}(t)$, $\hat{\vartheta}(t)$, and $\hat{\sigma}(t)$, then feeds them back to the L1-ANDI controller to adjust the system. Besides, while the adaptive law accurately estimates the impact of disturbances, it also ensures system stability. The projection operator $Proj(\cdot,\cdot)$ is defined before designing the adaptive law [29].

Definition 1 Consider a convex compact set defined by

$$\Omega_C = \left\{ \mu \in \mathbb{R}^n, \mu_i^{\min} \le \mu_i \le \mu_i^{\max} \right\}$$

where $\mu_i^{\max}$and $\mu_i^{\min}$ are upper and lower bounds for the i-th component of the μ. ε is a sufficiently small positive constant satisfied $\mu_i^{\min} + \varepsilon \le \mu_i \le \mu_i^{\max} - \varepsilon, \mu_i \in \Omega_C$. Then, the projection operator is defined by

$$\mathrm{Proj}(\mu, y) \triangleq \begin{cases} \frac{\mu_i^{\max} - \mu_i}{\varepsilon} y_i \ if \mu_i > \mu_i^{\max} - \varepsilon, and\ y_i > 0 \\ \frac{\mu_i - \mu_i^{\min}}{\varepsilon} y_i \ if \mu_i < \mu_i^{\min} + \varepsilon, and\ y_i < 0 \\ \\ y_i \qquad Otherwise \end{cases} \tag{18}$$

Recalling the projection operator, the adaptive law is designed as follows:

$$\begin{cases} \dot{\hat{\lambda}}(t) = \Gamma \,\mathrm{Proj}\left(\hat{\lambda}(t), -e^T(t) P G(x) u_{L1}(t)\right), \hat{\lambda}(0) = \hat{\lambda}_0 \\ \dot{\hat{\sigma}}(t) = \Gamma \,\mathrm{Proj}\left(\hat{\sigma}(t), -e^T(t) P G(x)\right), \quad \hat{\sigma}(0) = \hat{\sigma}_0 \\ \dot{\hat{\vartheta}}(t) = \Gamma \,\mathrm{Proj}\left(\hat{\vartheta}(t), -e^T(t) P G(x) x(t)\right), \quad \hat{\vartheta}(0) = \hat{\vartheta}_0 \end{cases} \tag{19}$$

In the adaptive law, $\Gamma \in R^+$ is adaptation gain, the symmetric positive definite matrix $P = P^T > 0$is the solution of the Lyapunov function $A_m^T P + P A_m = -Q$. $Q = Q^T > 0$ is also a symmetric positive definite matrix.$e(t)$ represents the error between the system and the state predictor.

$$e(t) = \hat{x}(t) - x(t) \tag{20}$$

The above structure reveals that the L1 adaptive structure, as the compensation mechanism, enhances the robustness of the L1-ANDI controller, enabling the L1-ANDI to perceive and estimate the occurrence of disturbances and reduce the dependence of the model, thus solving the problem that NDI control lacks robustness to disturbances. Not only that, the L1-ANDI control approach also avoids system oscillations due to excessive adaptation gain by the introduction of the low-pass filter, thus alleviating the contradiction between robustness and fast adaptation in traditional adaptive control.

3.4 Stability analysis

Define some parameter errors used in the analysis.

$$\begin{aligned} \tilde{\lambda}(t) &= \hat{\lambda}(t) - \lambda \\ \tilde{\vartheta}(t) &= \hat{\vartheta}(t) - \vartheta(t) \\ \tilde{\sigma}(t) &= \hat{\sigma}(t) - \sigma(t) \end{aligned} \tag{21}$$

Next, define the boundary according to (5) and (7).

$$\Theta(\rho) \triangleq 4\left(1 + \vartheta_b^2 + \sigma_b^2 + \frac{\lambda_{\max}(P)}{\lambda_{\min}(Q)}\left(\vartheta_b d_\vartheta + \sigma_b d_\sigma\right)\right) \tag{22}$$

From (2), (11) and (17), the dynamic of tracking errors can be derived.

$$\begin{aligned}\dot{e}(t) &= A_m(t)e(t)\\ &+ G(x)\left(\tilde{\lambda}(t)u_{L1}(t) + \tilde{\vartheta}(t)\|x(t)\|_\infty + \tilde{\sigma}(t)\right)\end{aligned} \tag{23}$$

Selecting the Lyapunov function candidate:

$$\begin{aligned}&V\left(e(t), \tilde{\lambda}(t), \tilde{\vartheta}(t), \tilde{\sigma}(t)\right)\\ &= e^T(t)Pe(t) + \Gamma^{-1}\left(\tilde{\vartheta}^T(t)\tilde{\vartheta}(t) + \tilde{\sigma}^T(t)\tilde{\sigma}(t)\right)\\ &\quad + \Gamma^{-1}trace\left(\tilde{\lambda}^T(t)\tilde{\lambda}(t)\right)\end{aligned} \tag{24}$$

At the initial time$t=0$, the function satisfies the boundary conditions:

$$V(0) \le \frac{4}{\Gamma}\left(1 + \vartheta_b^2 + \sigma_b^2\right) \le \frac{\Theta(\rho)}{\Gamma} \tag{25}$$

Combined with (23) yields

$$\begin{aligned}\dot{V}(t) &= 2e^T(t)P\dot{e}(t) + \frac{2}{\Gamma}\left(\tilde{\vartheta}^T(t)\dot{\tilde{\vartheta}}(t) + \tilde{\sigma}^T(t)\dot{\tilde{\sigma}}(t)\right)\\ &\quad + \frac{2}{\Gamma}trace\left(\tilde{\lambda}^T(t)\dot{\tilde{\lambda}}(t)\right)\\ &= -e^T(t)Qe(t) + \frac{2}{\Gamma}trace\left(\tilde{\lambda}^T(t)\left(\dot{\hat{\lambda}}(t) - \dot{\lambda}(t)\right)\right)\\ &\quad + \frac{2}{\Gamma}\tilde{\sigma}^T(t)\left(\dot{\hat{\sigma}}(t) - \dot{\sigma}(t)\right) + \frac{2}{\Gamma}\tilde{\vartheta}^T(t)\left(\dot{\hat{\vartheta}}(t) - \dot{\vartheta}(t)\right)\\ &\quad + 2e^T(t)PG(x)\left(\tilde{\lambda}(t)u_{L1}(t) + \tilde{\vartheta}(t)\|x(t)\|_\infty + \tilde{\sigma}(t)\right)\end{aligned} \tag{26}$$

For$\forall t \in [0,\tau)$, the substitution of the projection operator-based adaptive law (19) into the Eq. (26) leads to

$$\begin{aligned}\dot{V}(t) &= -e^T(t)Qe(t) - \frac{2}{\Gamma}\left(trace\left(\tilde{\lambda}^T(t)\dot{\lambda}(t)\right)\right.\\ &\quad \left. + \tilde{\sigma}^T(t)\dot{\sigma}(t) + \tilde{\vartheta}^T(t)\dot{\vartheta}(t)\right)\\ &\le -e^T(t)Qe(t) + \frac{2}{\Gamma}\left|\tilde{\sigma}^T(t)\dot{\sigma}(t) + \tilde{\vartheta}^T(t)\dot{\vartheta}(t)\right|\\ &\le -e^T(t)Qe(t) + \frac{4}{\Gamma}\left(\vartheta_b d_\vartheta + \sigma_b d_\sigma\right)\end{aligned} \tag{27}$$

From the boundary constraint in *Assumption 4*, we can obtain

$$\begin{aligned}&\max_{t\in[0,\tau)}\left(trace\left(\tilde{\lambda}^T(t)\tilde{\lambda}(t)\right) + \tilde{\vartheta}^T(t)\tilde{\vartheta}(t) + \tilde{\sigma}^T(t)\tilde{\sigma}(t)\right)\\ &\le 4\left(1 + \vartheta_b^2 + \sigma_b^2\right)\end{aligned} \tag{28}$$

Assume the existence of an arbitrary moment$\tau' \in (0,\tau)$ such that $V(\tau') > \frac{\Theta(\rho)}{\Gamma}$. Then, it follows from Eqs. (22), (24), and (28) that

$$e^T(\tau')Pe(\tau') > \frac{4}{\Gamma}\frac{\lambda_{\max}(P)}{\lambda_{\min}(Q)}\left(\vartheta_b d_\vartheta + \sigma_b d_\sigma\right) \tag{29}$$

Based on the knowledge between matrix eigenvalues and norm, the following inequalities hold:

$$\begin{aligned}\lambda_{\min}(Q)\|e(t)\|^2 \le e^TQe \le \lambda_{\max}(Q)\|e(t)\|^2\\ \lambda_{\min}(P)\|e(t)\|^2 \le e^TPe \le \lambda_{\max}(P)\|e(t)\|^2\end{aligned} \tag{30}$$

where the $\lambda_{\min}(\cdot)$ and $\lambda_{\max}(\cdot)$ represent the minimum and maximum eigenvalues of the matrix. Hence, Eq. (29) is deformed as follows

$$\begin{aligned}e^T(\tau')Qe(\tau') &\ge \frac{\lambda_{\min}(Q)}{\lambda_{\max}(P)}e^T(\tau')Pe(\tau')\\ &> \frac{4}{\Gamma}\left(\vartheta_b d_\vartheta + \sigma_b d_\sigma\right)\end{aligned} \tag{31}$$

When $V(\tau') > \frac{\Theta(\rho)}{\Gamma}$, conbining with Eq. (26), we can deduce that

$$\dot{V}(\tau') < 0 \tag{32}$$

Therefore, the Lyapunov function (24) satisfies (33) for all time.

$$V(t) \le \frac{\Theta(\rho)}{\Gamma}, t \in [0,\tau) \tag{33}$$

Due to $V(t) \ge e^T(t)Pe(t) \ge \lambda_{\min}(P)\|e(t)\|_2^2$, yields

$$\|e(t)\|_\infty^2 \le \|e(t)\|_2^2 \le \frac{\Theta(\rho)}{\lambda_{\min}(P)\Gamma} \tag{34}$$

In conclusion, the bounds of system tracking errors are as follows

$$\|e(t)\|_\infty \le \sqrt{\frac{\Theta(\rho)}{\lambda_{\min}(P)\Gamma}} \tag{35}$$

The above derivation further demonstrates that the projection operator-based adaptive law ensures system stability and maintains the tracking errors within a uniform bound. Since the bound is inversely proportional to the square root of the adaptation gain, increasing the adaptation gain is an effective way to narrow the bound of the errors.

The reference system in Eqs. (36)–(39) is introduced to further analyze the dynamic performance of the L1-ANDI controller.

$$\dot{x}_{ref}(t) = f\left(x_{ref}\right) + G\left(x_{ref}\right)\begin{pmatrix}\lambda u_{NDI,ref}(t) + \lambda u_{L1,ref}(t)\\ + \vartheta(t)\left\|x_{ref}(t)\right\|_\infty + \sigma(t)\end{pmatrix} \tag{36}$$

$$u_{NDI,ref}(t) = \left(G\left(x_{ref}\right)\lambda\right)^{-1}\left(v_{ref} - f\left(x_{ref}\right)\right) \tag{37}$$

$$v_{ref} = A_m\left(x_{ref}(t) - x_{cmd}(t)\right) \tag{38}$$

$$u_{L1,ref}(s) = -\frac{C(s)}{\lambda}\left(\vartheta(s)\left\|x_{ref}(s)\right\|_{\infty} + \sigma(s)\right) \tag{39}$$

In practice, this reference system is a virtual system, which defines the expected performance that the system can achieve. The reference system is thus only used for analysis purposes.

Under the $u_{NDI,\,ref}$, the reference system becomes:

$$\begin{aligned}\dot{x}_{ref}(t) &= A_m x_{ref} - A_m x_{cmd} \\ &+ G\left(x_{ref}\right)\left(\lambda u_{L1,ref}(t) + \vartheta(t)\left\|x_{ref}(t)\right\|_{\infty} + \sigma(t)\right)\end{aligned} \tag{40}$$

Further, under the action of the L1 controller $u_{L1,\,ref}$, the reference system closed-loop dynamics are as follows:

$$\begin{aligned}x_{ref}(s) &= \left(sI - A_m\right)^{-1}\left(-A_m\right)x_{cmd} \\ &+ (I - C(s))\left(\vartheta(t)\left\|x_{ref}(s)\right\|_{\infty} + \sigma(s)\right)\end{aligned} \tag{41}$$

Since $C(0) = 1$ and A_m is the Hurwitz matrix, then applying the final value theorem in a closed-loop reference system in the case of constant $x_{cmd}(t) \equiv x_{cmd}$, yields $\lim_{t\to\infty} x_{ref}(t) = x_{cmd}$, the reference system is stable and achieves the desired dynamics.

Since the reference system subjects to the L1-norm condition (16), it can be deduced that

$$\left\|x_{ref} - x\right\|_{L_\infty} \le \frac{\gamma_1}{\sqrt{\Gamma}}, \left\|u_{L1,ref} - u_{L1}\right\|_{L_\infty} \le \frac{\gamma_2}{\sqrt{\Gamma}} \tag{42}$$

where

$$\begin{aligned}\gamma_1 &\triangleq \frac{\|C(s)\|_{L_1}}{1 - \|\Phi(s)(1 - C(s))\|_{L_1}\vartheta_b}\sqrt{\frac{\Theta(\rho)}{\lambda_{\min}(P)}} \\ \gamma_2 &\triangleq \left\|\frac{C(s)}{\lambda}\right\|_{L_1}\vartheta_b\gamma_1 + \left\|\frac{C(s)\Phi^{-1}(s)}{\lambda}\right\|_{L_1}\sqrt{\frac{\Theta(\rho)}{\lambda_{\min}(P)}} \\ \Phi(s) &\triangleq (^sI - A_m)^{-1}G(x)\end{aligned} \tag{43}$$

Proof For clarity, define some variables used in the proof process.

$$H_1(s) \triangleq \Phi(s)(1 - C(s)) \tag{44}$$

$$H_2(s) \triangleq \Phi(s)C(s) \tag{45}$$

Combining Eq. (39), the state dynamics of the reference system can be converted to the frequency domain form, as follows:

$$x_{ref}(s) = H_1(s)\eta_{ref}(s) - \left(sI - A_m\right)^{-1}A_m x_{cmd}(s) \tag{46}$$

where $\eta_{ref}(s) \triangleq \vartheta(s)\|x_{ref}(s)\|_{\infty} + \sigma(s)$.

Based on Eqs. (15) and (21), the L1 adaptive controller (13) can be transformed into

$$u_{L1}(s) = -\frac{C(s)}{\lambda}\left(\eta(s) + \tilde{\eta}(s)\right) \tag{47}$$

where

$$\begin{aligned}\tilde{\eta}(s) &\triangleq \tilde{\lambda}(s)u_{L1}(s) + \tilde{\vartheta}(s)\|x(s)\|_{\infty} + \tilde{\sigma}(s) \\ \eta(s) &\triangleq \vartheta(s)\|x(s)\|_{\infty} + \sigma(s)\end{aligned} \tag{48}$$

Under the action of control law (12) and (47), the frequency domain form of the system (2) can be written as:

$$x(s) = H_1(s)\eta(s) - H_2(s)\tilde{\eta}(s) - \left(sI - A_m\right)^{-1}A_m x_{cmd}(s) \tag{49}$$

Thus, the dynamic error between the reference system and the actual system can be deduced as follows:

$$x_{ref}(s) - x(s) = H_1(s)\left(\eta_{ref}(s) - \eta(s)\right) + H_2(s)\tilde{\eta}(s) \tag{50}$$

It can be deduced from Eq. (23) that

$$\tilde{\eta}(s) = \Phi^{-1}(s)e(s) \tag{51}$$

The upper bound of Eq. (50) can be expressed as

$$\begin{aligned}\left\|\left(x_{ref} - x\right)_{\tau}\right\|_{L_\infty} &\le \left\|H_1(s)\right\|_{L_1}\left\|\left(\eta_{ref} - \eta\right)_{\tau}\right\|_{L_\infty} \\ &+ \left\|H_2(s)\Phi^{-1}(s)\right\|_{L_1}\left\|e_{\tau}\right\|_{L_\infty}\end{aligned} \tag{52}$$

According to the bounded condition in Eq. (7), it follows that

$$\left\|\left(\eta_{ref} - \eta\right)_{\tau}\right\|_{L_\infty} \le \vartheta_b\left\|\left(x_{ref} - x\right)_{\tau}\right\|_{L_\infty} \tag{53}$$

Further, substituting Eqs. (35) and (53) into Eq. (52), yields:

$$\left\|\left(x_{ref} - x\right)_{\tau}\right\|_{L_\infty} \le \frac{\|C(s)\|_{L_1}}{1 - \left\|H_1(s)\right\|_{L_1}\vartheta_b}\sqrt{\frac{\Theta(\rho)}{\lambda_{\min}(P)\Gamma}} \tag{54}$$

which holds uniformly for all $\tau \ge 0$, leading to $\left\|x_{ref} - x\right\|_{L_\infty} \le \frac{\gamma_1}{\sqrt{\Gamma}}$.

Similarly, the dynamic error between $u_{L1,\,ref}(s)$ and $u_{L1}(s)$ can be expressed as follows:

$$u_{L1,ref}(s) - u_{L1}(s) = -\frac{C(s)}{\omega}\left(\eta_{ref}(s) - \eta(s)\right) + \frac{C(s)}{\omega}\tilde{\eta}(s) \tag{55}$$

Referring to the Lemma A.12.1 in Ref [28] and combining in equations (53) and (54), one obtains:

$$\begin{aligned}\left\|\left(u_{ref} - u\right)_{\tau}\right\|_{L_\infty} &\le \left\|\frac{C(s)}{\omega}\right\|_{L_1}\vartheta_b\gamma_1 + \left\|\frac{C(s)\Phi^{-1}(s)}{\omega}\right\|_{L_1}\sqrt{\frac{\Theta(\rho)}{\lambda_{\min}(P)\Gamma}} \\ &= \gamma_2\end{aligned} \tag{56}$$

The proof is complete.

Remark 3 The in equation (42) indicates that by increasing the adaptive gain Γ, the performance of the actual system (2) in ideal conditions can be arbitrarily close to that of a reference system with the desired performance. In practice, despite the presence of the low-pass filter, the adaptive gain cannot be infinite. Therefore, increasing the adaptive gain within the hardware limits is capable of reducing the tracking error and improving the control performance.

4 Flight Controller Design

This section establishes the 6-degrees of freedom aircraft model with CG variations and designs the flight controller based on the proposed L1-ANDI approach.

4.1 Aircraft modeling with CG variations

To develop the aircraft dynamic model, this paper utilizes the CATIA software to design the aircraft model, and aerodynamic coefficients are calculated through the Xflow software.

In the process of aircraft modeling, the effect of the CG variations must be taken into account. Assume that the aircraft is a rigid body, the ground reference frame is regarded as an inertial frame, and the origin of the body-fixed frame O is also the location of the original CG of the aircraft. The position of CG deviates from the original position, as shown Fig. 1.

In Fig.1, $O^{'}$ represents the current CG in the body-fixed frame.$\Delta r=[\Delta x_{cg},\Delta y_{cg},\Delta z_{cg}]^T$ is the CG offset with respect to the original CG. According to Ref [30], the force and moment equations of an aircraft with CG variations are described as

$$\begin{aligned} X &= m\Big[\dot{u}-rv+qw-\left(q^2+r^2\right)\Delta x_{cg}+(pq-\dot{r})\Delta y_{cg} \\ &\quad +(pr+\dot{q})\Delta z_{cg}+g\sin\theta\Big] \\ Y &= m\Big[\dot{v}+ru-pw+(pq+\dot{r})\Delta x_{cg}-\left(p^2+r^2\right)\Delta y_{cg} \\ &\quad +(qr-\dot{p})\Delta z_{cg}-g\cos\theta\sin\phi\Big] \\ Z &= m\Big[\dot{w}+pv-qu+(pr-\dot{q})\Delta x_{cg}+(qr+\dot{p})\Delta y_{cg} \\ &\quad -\left(p^2+q^2\right)\Delta z_{cg}-g\cos\theta\cos\phi\Big] \end{aligned} \tag{57}$$

$$\begin{aligned} L &= I_{xx}\dot{p}-I_{xy}\dot{q}-I_{xz}\dot{r}+I_{xy}pr-I_{xz}pq+\left(I_{zz}-I_{yy}\right)qr \\ &\quad +I_{yz}\left(r^2-q^2\right)+m\left((\dot{w}-qu+pv)\Delta y_{cg}-(\dot{v}+ru-pw)\Delta z_{cg}\right) \\ M &= -I_{xy}\dot{p}+I_{yy}\dot{q}-I_{yz}\dot{r}+I_{yz}pq-I_{xy}qr+\left(I_{xx}-I_{zz}\right)qr \\ &\quad +I_{xz}\left(p^2-r^2\right)+m\left((\dot{u}-rv+qw)\Delta z_{cg}-(\dot{w}+pv-qu)\Delta x_{cg}\right) \\ N &= -I_{xz}\dot{p}-I_{yz}\dot{q}+I_{zz}\dot{r}-I_{yz}pr+I_{xz}qr+\left(I_{yy}-I_{xx}\right)pq \\ &\quad +I_{xy}\left(q^2-p^2\right)+m\left((\dot{v}+ru-pw)\Delta x_{cg}-(\dot{u}-rv+qw)\Delta y_{cg}\right) \end{aligned} \tag{58}$$

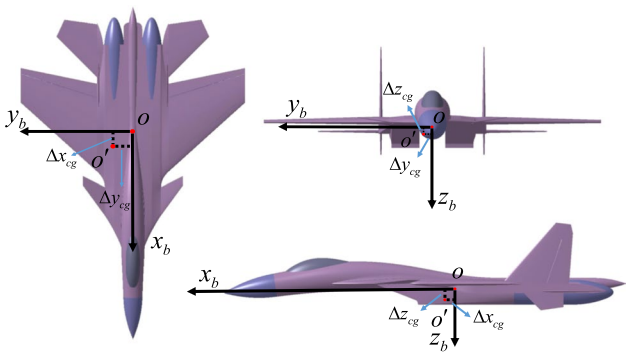

Fig. 1 The change of the CG diagram

where $F=[X,Y,Z]^T$ is the sum of forces except for gravity, and $\overline{M}=[L,M,N]^T$is the total moments, which are all expressed in the body-fixed frame. m is the mass of the aircraft. g is the gravity acceleration. θ and $\phi$are pitch angle and roll angle. Both $\omega=[p,q,r]^T$and $v_0=[u,v,w]^T$are the angular rate and the velocity vectors relative to the original CG. Additionally, the inertia matrix is as follows

$$J=\begin{bmatrix} I_{xx} & -I_{xy} & -I_{xz} \\ -I_{xy} & I_{yy} & -I_{yz} \\ -I_{xz} & -I_{yz} & I_{zz} \end{bmatrix} \tag{59}$$

$$\begin{aligned} \dot{\omega} &= J^{-1}\left(\overline{M}-\omega\times J\omega-\Delta r\Omega v_b-\Delta r\dot{v}_b\right) \\ \dot{v}_b &= \left(F+G_b\right)/m-\left(\omega\times v_b+\gamma\Delta r\right) \end{aligned} \tag{60}$$

where

$$\Delta r=\begin{bmatrix} 0 & -m\Delta z & m\Delta y \\ m\Delta z & 0 & -m\Delta x \\ -m\Delta y & m\Delta x & 0 \end{bmatrix}, G_b=mg\begin{bmatrix} \sin\theta \\ -\cos\theta\sin\phi \\ -\cos\theta\cos\phi \end{bmatrix}$$
$$\gamma=\begin{bmatrix} -q^2-r^2 & pq-\dot{r} & pr+\dot{q} \\ pq+\dot{r} & -p^2-r^2 & qr-\dot{p} \\ pr-\dot{q} & qr+\dot{p} & -p^2-q^2 \end{bmatrix}, \Omega=\begin{bmatrix} 0 & -r & q \\ r & 0 & -p \\ -q & p & 0 \end{bmatrix}$$

When the CG does not change, the CG location is at the origin of the body-fixed frame, that is, $\Delta r=0$ and the coss-products of inertia $I_{yz}=0$ and $I_{xy}=0$. The lateral and longitudinal motions of aircraft are decoupled. After the CG shift, the Δr, I_{yz}, and I_{xy} undergo variations. Equations (57), (58), and (60) indicate that the CG shift creates additional forces and moments for aircraft, which introduces undesirable coupling between longitudinal and lateral motions, and that these unexpected effects must be compensated by the flight controller.

The forces due to manipulation and aerodynamics are

$$\begin{aligned} X &= \overline{Q}SC_X\left(M_a,\alpha,\beta,q,\delta_e\right)+\delta_{th}T_{\max}\\ Y &= \overline{Q}SC_Y\left(M_a,\alpha,\beta,p,r,\delta_a,\delta_r\right)\\ Z &= \overline{Q}SC_Z\left(M_a,\alpha,\beta,q,\delta_e\right) \end{aligned} \tag{61}$$

where $\overline{Q}$ is the dynamic pressure, S is the wing area, M_a is the Mach number, $T_{\max}$is the maximum thrust of the engine. α and β are the angle of attack and sideslip angle, respectively. Elevator δ_e, aileron δ_a, rudder δ_r, and throttle δ_{th} are used as control devices.

To highlight the role of the control surface, the moments can be further divided into

$$\begin{bmatrix} L\\ M\\ N \end{bmatrix} = \overline{Q}S\left(\begin{bmatrix} bC_l^*\\ \overline{c}C_m^*\\ bC_n^* \end{bmatrix}+\begin{bmatrix} bC_{l\delta_a} & 0 & bC_{l\delta_r}\\ 0 & \overline{c}C_{m\delta_e} & 0\\ bC_{n\delta_a} & 0 & bC_{n\delta_r} \end{bmatrix}\begin{bmatrix} \delta_a\\ \delta_e\\ \delta_r \end{bmatrix}\right) \tag{62}$$

where b is the wingspan, and $\overline{c}$ is the mean aerodynamic chord. C_l^*, C_m^*, and C_n^* are the moment coefficients except for manipulation terms. Besides, $C_{m\delta_e}$,$C_{l\delta_a}$,$C_{n\delta_a}$,$C_{l\delta_r}$, and $C_{n\delta_r}$ are the manipulation coefficients. So the second term represents the control surface manipulation terms.

All aerodynamic and control coefficients in Eqs. (61)–(62) are calculated by Xflow software. The sum of force and moment coefficients excluding manipulation and dynamic coefficients are described in Fig. 2.

Additionally, the dynamics of the angles of attack, sideslip angle, and roll angle are expressed as follows:

$$\begin{bmatrix} \dot{\alpha}\\ \dot{\beta}\\ \dot{\phi} \end{bmatrix} = S_1\begin{bmatrix} p\\ q\\ r \end{bmatrix}+\frac{1}{mV_a}S_2\left(\begin{bmatrix} X\\ Y\\ Z \end{bmatrix}+mg\begin{bmatrix} sin\theta\\ -cos\theta sin\phi\\ -cos\theta cos\phi \end{bmatrix}\right) \tag{63}$$

with

$$\begin{aligned} S_1 &= \begin{bmatrix} -\tan\beta\cos\alpha & 1 & -\tan\beta\sin\alpha\\ \sin\alpha & 0 & -\cos\alpha\\ 1 & \tan\theta\sin\phi & \tan\theta\cos\phi \end{bmatrix}\\ S_2 &= \begin{bmatrix} -\sin\alpha/\cos\beta & 0 & \cos\alpha/\cos\beta\\ -\cos\alpha\sin\beta & \cos\beta & -\sin\alpha\sin\beta\\ 0 & 0 & 0 \end{bmatrix} \end{aligned} \tag{64}$$

where V_a is the airspeed, as follows:

$$V_a = \left\|v_b\right\|_2 = \sqrt{u^2+v^2+w^2} \tag{65}$$

4.2 Control architecture

For the aircraft that control moment produced by traditional aerodynamic control surfaces, it is reasonable

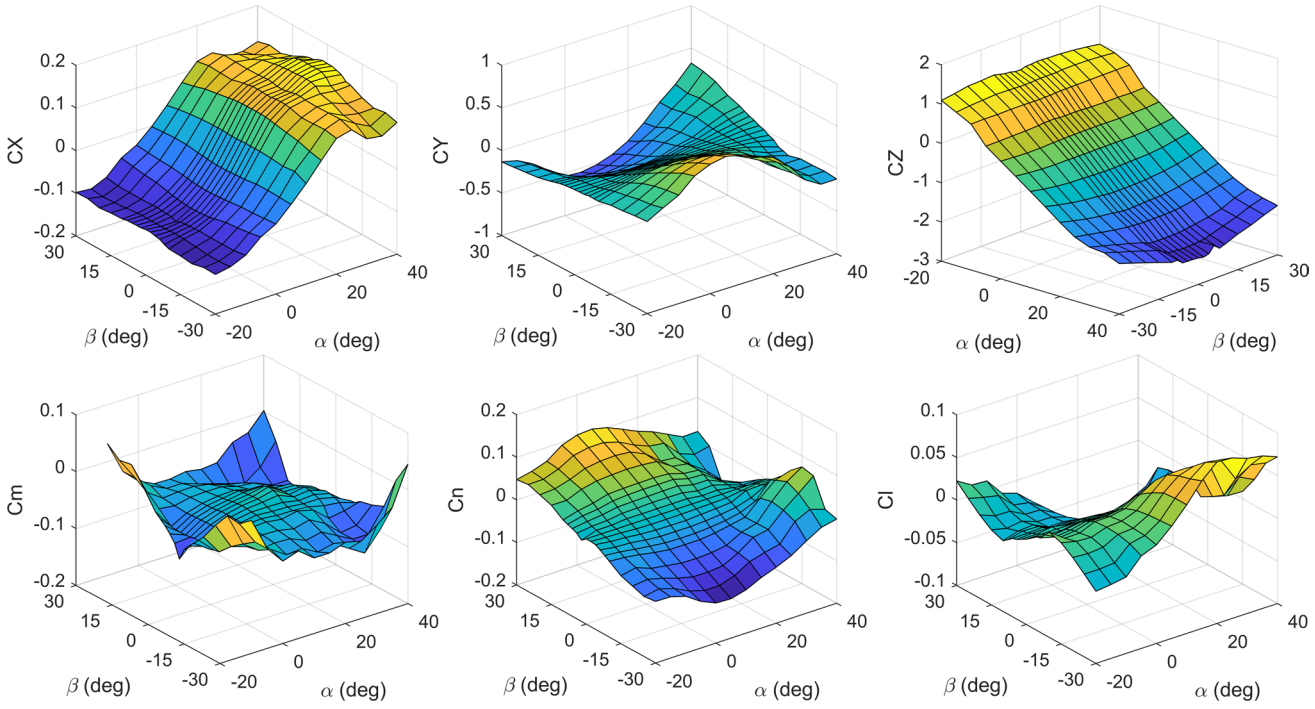

Fig. 2 The surface figure of forces and moments coefficient excluding manipulation and dynamic coefficients

to assume that rotational dynamics are always faster than translational dynamics. Based on the timescale separation principle [31], multiple states can be decoupled into two cascaded structures, detail as follows

$$\begin{aligned} \dot{x}_1 &= f_1(x) + G_1(x)u + \xi \\ \dot{x}_2 &= f_2(x) + G_2(x)x_1 \end{aligned} \tag{66}$$

Due to the relatively fast dynamics, the angular rates are classified into the inner loop ($x_1 = \omega$), while the angles of attack, sideslip angle, and roll angle are classified as the outer loop ($x_2 = [\alpha, \beta, \phi]^T$). So

$$\begin{aligned} f_1(x) &= J^{-1}\left(\overline{Q}S\begin{bmatrix} bC_l^* \\ \bar{c}C_m^* \\ bC_n^* \end{bmatrix} - \begin{bmatrix} p \\ q \\ r \end{bmatrix} \times J\begin{bmatrix} p \\ q \\ r \end{bmatrix}\right) \\ G_1(x) &= J^{-1}\overline{Q}S\begin{bmatrix} bC_{l\delta_a} & 0 & bC_{l\delta_r} \\ 0 & \bar{c}C_{m\delta_e} & 0 \\ bC_{n\delta_a} & 0 & bC_{n\delta_r} \end{bmatrix} \\ \xi &= -J^{-1}\left(\Delta r \Omega v_b + \Delta r \dot{v}_b\right), u = \begin{bmatrix} \delta_a, \delta_e, \delta_r \end{bmatrix}^T \\ f_2(x) &= \frac{1}{mV_a}S_2\left(\begin{bmatrix} X \\ Y \\ Z \end{bmatrix} + mg\begin{bmatrix} \sin\theta \\ -\cos\theta\sin\phi \\ -\cos\theta\cos\phi \end{bmatrix}\right) \\ G_2(x) &= S_1 \end{aligned} \tag{67}$$

In the cascaded structure, command signals are given to the outer loop, outputs of the outer loop are regarded as the reference signals of the inner loop, and outputs of the inner loop are used as the commands of control surfaces. In order to overcome disturbances and coupling effects caused by the CG shift and achieve the desired dynamic performance, the L1-ANDI control approach is utilized to design the angular rate controller, and the Integral NDI technique is used to design the outer loop controller.

4.3 L1-ANDI-based flight controller

The relationship between states of the outer loop ($x_2 = [\alpha, \beta, \phi]^T$) and angular rates are clear, so the NDI strategy aforementioned in the Eq. (8) is employed to design the outer loop controller. Combining the Eq. (63), the Integral NDI-based outer loop controller is designed as follows

$$\begin{bmatrix} p_{cmd} \\ q_{cmd} \\ r_{cmd} \end{bmatrix} = {S_1}^{-1}\left(\begin{bmatrix} \dot{\alpha}_{des} \\ \dot{\beta}_{des} \\ \dot{\phi}_{des} \end{bmatrix} - f_2(x)\right) \tag{68}$$

where the definitions of S_1 and $f_2(x)$ are described in the previous Eq. (67). $\dot{x}_{2,des} = \left[\dot{\alpha}_{des}, \dot{\beta}_{des}, \dot{\phi}_{des}\right]^T$ represents the desired dynamics of x_2. To maintain the satisfactory tracking performance, it adopts the proportional-integral strategy to achieve second-order error dynamics with frequencies and damping ratios, as follows

$$\begin{bmatrix} \dot{\alpha}_{des} \\ \dot{\beta}_{des} \\ \dot{\phi}_{des} \end{bmatrix} = K_P e_{x_2} + \frac{K_I}{s} e_{x_2} \tag{69}$$

with

$$\begin{aligned} e_{x_2} &= \begin{bmatrix} \alpha_{cmd} \\ \beta_{cmd} \\ \phi_{cmd} \end{bmatrix} - \begin{bmatrix} \alpha \\ \beta \\ \phi \end{bmatrix} \\ K_P &= \mathrm{diag}\left(2\xi_\alpha\omega_\alpha, 2\xi_\beta\omega_\beta, 2\xi_\phi\omega_\phi\right) \\ K_I &= \mathrm{diag}\left({\omega_\alpha}^2, {\omega_\beta}^2, {\omega_\phi}^2\right) \end{aligned} \tag{70}$$

Similarly, the desired inner control loop dynamics ν_{des} are as follows

$$\nu_{des} = \begin{bmatrix} \dot{p}_{des} \\ \dot{q}_{des} \\ \dot{r}_{des} \end{bmatrix} = A_m\left(\begin{bmatrix} p \\ q \\ r \end{bmatrix} - \begin{bmatrix} p_{cmd} \\ q_{cmd} \\ r_{cmd} \end{bmatrix}\right) \tag{71}$$

with

$$A_m = -\mathrm{diag}\left(\omega_p, \omega_q, \omega_r\right) \tag{72}$$

where ω_p,ω_q, and ω_r are the bandwidth of angular rates.

It is clear from the Eq. (66) that the CG shift introduces undesired moments, which severely affect the angular rate dynamics. Therefore, the L1-ANDI control approach proposed in Section 3 is employed to design the angular rate controller, whose structure is referred to Eqs. (11)–(13), and the state predictor and adaptive law are consistent with Eqs. (17) and (19). The overall flight control architecture is schematized in Fig. 3. In the structure of the L1-ANDI controller, the transfer function is selected as $D(s) = 1/s$ and the filter gain is chosen as $K_D = 20$. The adaptive gains are set as $\Gamma = 400$, and the $Q = diag(2, 5, 10)$ for the Lyapunov function. Additionally, Table 1 lists the outer loop and inner loop dynamic parameters.

5 Simulation and Analysis

To illustrate and assess the dynamic performance and robustness of the L1-ANDI-based flight controller, a series of simulations are performed in the Matlab/Simulink. For the sake of fairness, the proposed L1-ANDI control approach is also compared with the L1, MRAC, ANDI, and conventional NDI control methods.

All simulation experiments are carried out around the cruise condition with $V_a = 80m/s$,$H = 500m$, and $\alpha = \theta = 3.5deg$. The dynamics of actuators for all control surfaces are considered and modeled by the first-order transfer function. The structure is described in Fig. 4.

In Fig. 4, K_ω represents the bandwidth. The limitations of actuators are shown in Table 2.

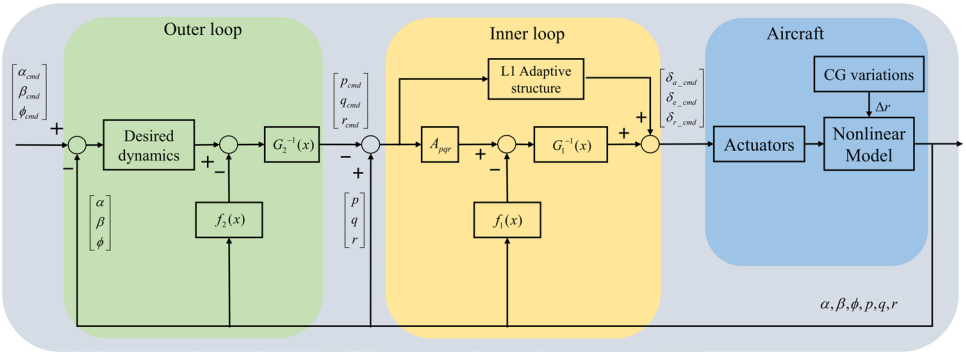

Fig. 3 The overall framework of flight control law based on the L1-ANDI approach

Table 1 The flight controller parameters

Parameter	Value
$\omega_p\omega_q\omega_r$	10 rad/s
$\xi_\alpha\xi_\beta\xi_\phi$	$1/\sqrt{2}$
ω_α	1.1
ω_β	1
ω_ϕ	1.2

During the wing-level flight, the aircraft's CG is shifted from the original location at 12 s. Assuming that the shift is completed instantaneously and the displacement is $\Delta r = [0.2, 0.3, 0.25]^T$. The simulation results are shown in Figs. 5, 6 and 7.

The comparison results of angular rates and angles are shown in Figs. 5 and 6. The CG sudden shift breaks the balance of the aircraft, resulting in a sudden change in all states. The free-responses of the aircraft are terrible. In contrast, under the action of the L1-ANDI-based flight controller, the magnitudes of state changes are relatively small and acceptable, and the aircraft quickly returns to wing-level flight. Figure 7 describes the change of parameters estimated, from which it can be seen that the adaptive law begins to work immediately after the CG shift.

Next, the robustness of the L1-ANDI-based angular rate controller is verified by comparison. The comparisons are divided into two groups of the nonlinear controller and linear controller. Among them, the linear group includes L1-ANDI, L1, and MRAC controllers, and the nonlinear group consists of the L1-ANDI, ANDI, and NDI controllers. It is worth noting that for the sake of fairness, the adaptive gain in the L1-ANDI, L1, and MRAC controllers is chosen to be the same ($\Gamma = 400$), and the angular rate bandwidths (ω_p, ω_q, ω_r) in the L1-ANDI, ANDI, and NDI controllers are also selected to be the same, which ensures the dynamics of angular rate are consistent when the aircraft is not affected by disturbances.

The pitch and roll angle rate commands are given to aircraft, and the yaw angle rate is required to keep zero. Similarly, the aircraft suffers a CG sudden change at 12 s. The comparison results of the linear controller group are shown in Figs. 8, 9 and 10.

The results in Fig. 8 depict the angular rate comparison results under the L1-ANDI, L1, and MRAC robust flight controllers. In normal cases, all controllers achieve the same control performance, and angular rate dynamics satisfy the expected requirements. However, after suffering from the CG sudden shifts, the pitch, roll, and yaw angular rates under the MRAC controller all oscillated. Due to the presence of a low-pass filter, even at a high adaptive gain Γ, the L1-ANDI and L1 adaptive controllers eliminate the influence of high-frequency dynamics, thus avoiding oscillations while overcoming the disturbance. Therefore, under the action of the L1 and L1-ANDI flight controller, angular rates present fast evolutions without annoying oscillations, and their dynamics are still satisfactory. Nevertheless, in terms of transient

Table 2 Limitations of the actuators

Actuator	Bandwidth	Deflection limit	Rate limit
Aileron	60 rad	±21.5 rad/s	±80 rad/s
Elevator	60 rad	±25 rad/s	±60 rad/s
Rudder	60 rad	±30 rad/s	±70 rad/s

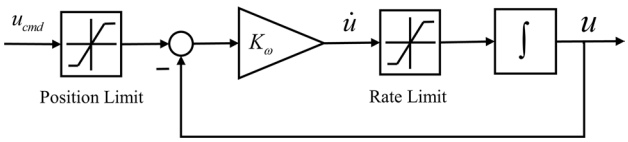

Fig. 4 The structure of the actuator

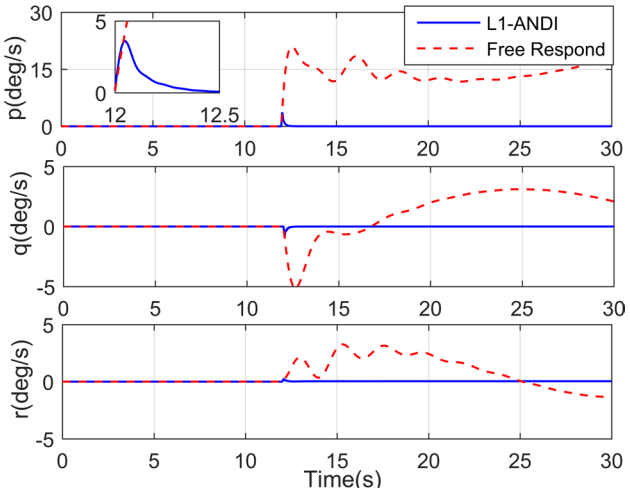

Fig. 5 Comparisons of angular rates

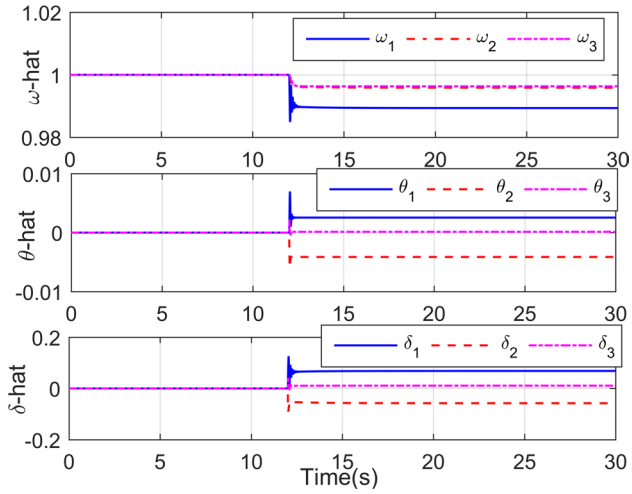

Fig. 7 Estimation results from the adaptive law

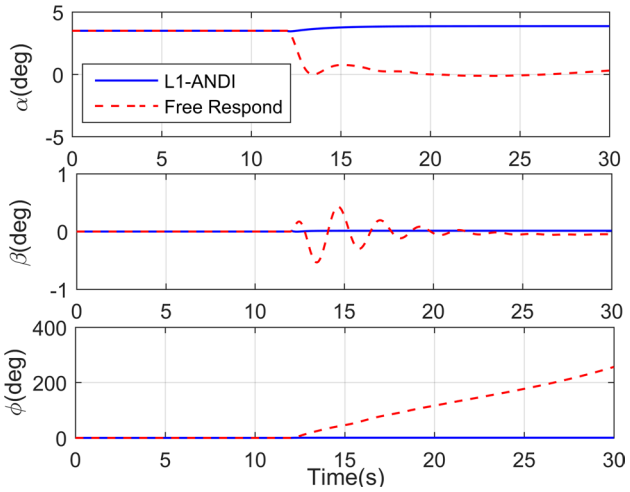

Fig. 6 Comparison results of attitude angles

dynamics, the angular rates under the L1-ANDI controller have a smaller overshoot, which is much superior to the L1 controller. The reason is that in addition to overcoming the disturbance of the CG sudden shifts, the L1 adaptive flight controller also needs to eliminate the nonlinearity caused by the aircraft state change, which can be demonstrated from the results of adaptive estimation in L1-ANDI, L1, and MRAC controllers depicted in Fig. 9.

In Fig. 9, the adaptive estimation of $\hat{\lambda}(t)$,$\hat{\vartheta}(t)$, and $\hat{\sigma}(t)$ in the MRAC and L1 adaptive flight controllers are significantly larger than that of the L1-ANDI, which means the change of its own nonlinear terms are regarded as the disturbance. Additionally, in the same adaptive gain, the high-frequency parts of the adaptive law estimation in MRAC control are the cause of angular rate oscillations.

Control surface deflections are shown in Fig. 10. In comparison, all control surfaces under the L1-ANDI and L1 flight controller are smoother. On the contrary, the elevator and aileron in the MRAC control oscillate due to the high adaptive gain, which is unacceptable.

With the same command signals and the disturbance of CG sudden shifts, the comparison results of the nonlinear controller group are shown in Figs. 11 and 12.

As shown in Fig. 11, the L1-ANDI, ANDI, and NDI flight controllers all achieve the same dynamic performance under normal conditions since the angular rate bandwidths are the same. The shift of CG introduces additional forces and moments, causing the aircraft model to no longer be accurate and bringing the longitudinal and lateral coupling. However, due to the lack of robustness, the control performance of NDI flight control is significantly degraded after the injection of CG shift, so angular rates deviate from their commands to a large extent. Conversely, with the action of the ANDI and L1-ANDI controllers, angular rates quickly re-track their commands. However, although the adjustment times of the L1-ANDI and ANDI controllers are the same and there are no annoying oscillations in the control surface deflections shown in Fig. 12, all angular rate overshoots under the L1-ANDI controller are smaller than that of the ANDI controller. After suffering from the CG sudden shifts, the coupling effect of pitch angular rate on roll angular rate is more pronounced with the ANDI controller than with the L1-ANDI controller, and the rapid of the roll angular rate under the ANDI controller is significantly slower than that of L1-ANDI. Therefore, the control performance of the L1-ANDI is more outstanding than that of traditional ANDI.

To further evaluate the control performance, the comparative simulation is carried out to compare the robustness of

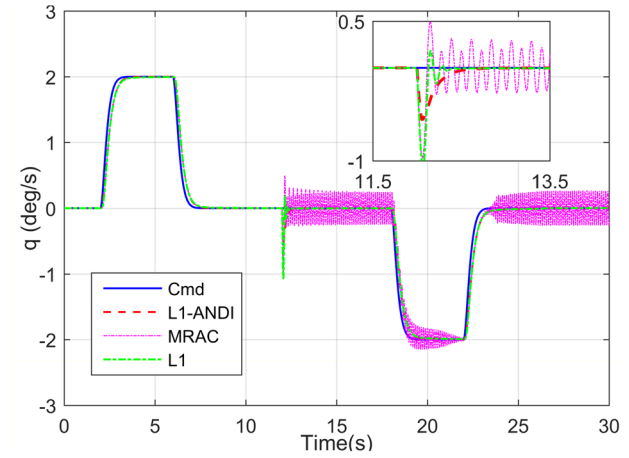

Fig. 8 Comparison results of angular rate under the L1-ANDI, MRAC, and L1 controllers (**a**) Pitch angular rate (**b**) Roll angular rate (**c**) Yaw angular rate

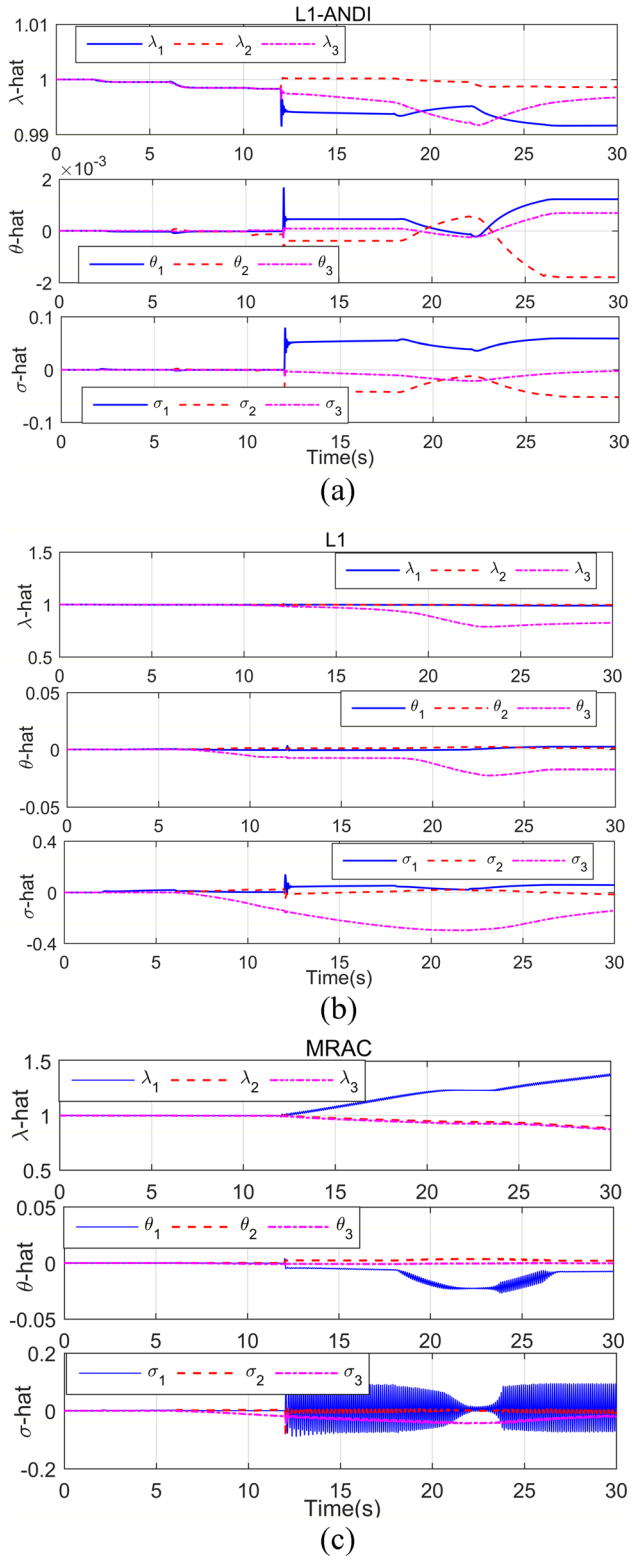

Fig. 9 Adaptive estimation results in L1-ANDI, L1, and MRAC controllers (**a**) Estimation results from the L1-ANDI controller (**b**) Estimation results from the L1 controller (**c**) Estimation results from the MRAC controller

the attitude angle controllers based on the L1-ANDI, L1, and NDI angular rate controllers as inner loops, respectively. The commands for the angle of attack and roll angle are

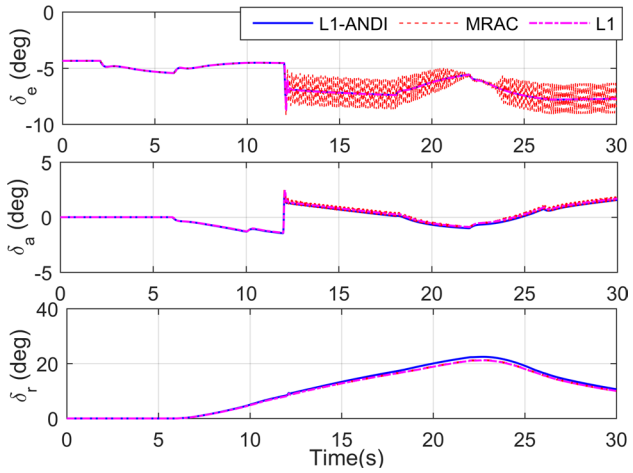

Fig. 10 Comparison results of control surface deflections

given while the sideslip angle is held at zero. Assuming the aircraft suffers a CG sudden shift at 6 s. Figure 13 shows the comparison results of angles of attack, sideslip angle, and roll angle, Fig. 14 shows the comparison results of angular rates, and Fig. 15 shows the comparison results of actuator deflections.

Similar to the previous results shown in Figs. 11 and 12, the control performance of the attitude controller with NDI-based angular rate controller as the inner loop is no longer satisfactory after the CG sudden shifts (6 seconds), resulting in large tracking errors in angles of attack, roll, and sideslip. Instead, both L1 and L1-ANDI controllers have the compensation mechanism that eliminates the adverse effects caused by the CG sudden shifts so that the attitude controllers with L1 and L1-ANDI angular rate controllers achieve expected dynamic performance. Since Fig. 8 indicates that the transient performance of the L1-ANDI controller is superior to the L1 adaptive controller. Therefore, compared with the attitude angle controller with the L1 adaptive controller as the inner loop, the attitude angle controller with the L1-ANDI controller as the inner loop has a smaller overshoot and adjustment time. The angular rates and control surface deflections depicted in Figs. 14 and 15 change smoothly and without oscillations.

In conclusion, the L1-ANDI control proposed in this paper is robust that is capable of eliminating the disturbance caused by the CG sudden shift. This approach inherits the fast decoupling capability and robustness from NDI and L1 adaptive control approaches, while solving the problems of model dependence in NDI control and the oscillation problem caused by a high adaptive gain.

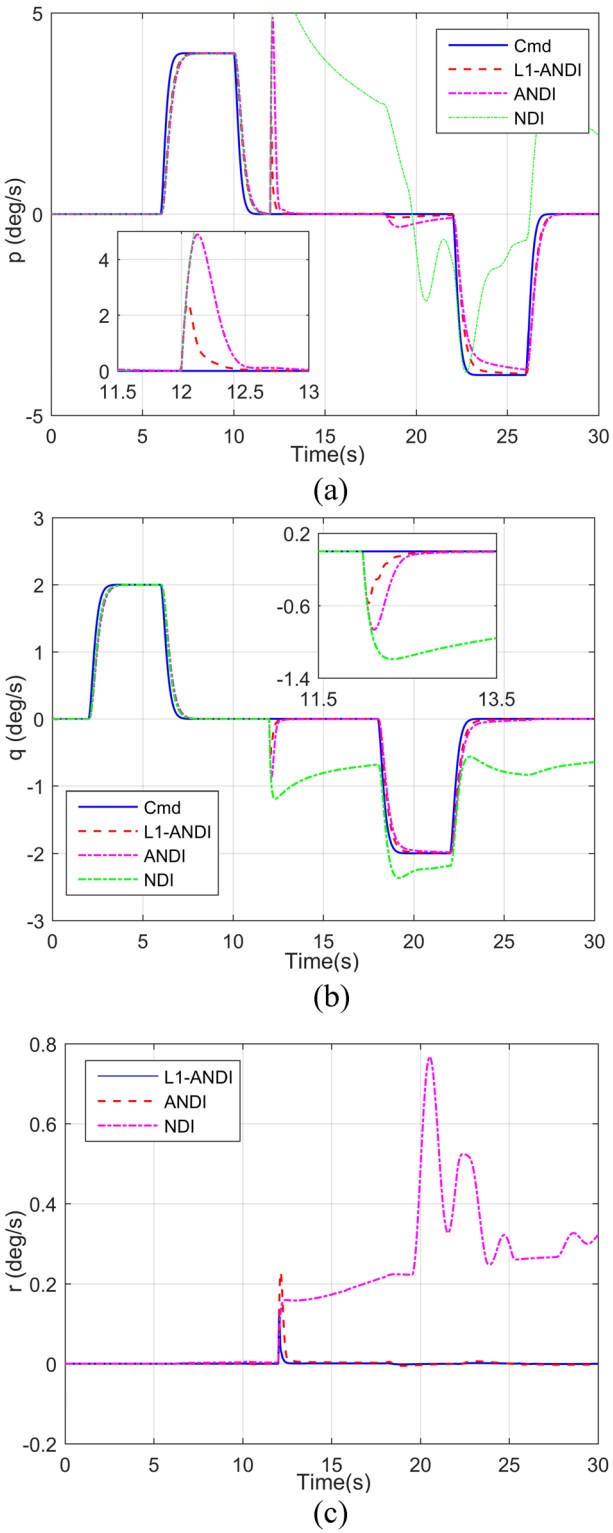

Fig. 11 Comparison results of angular rate under the L1-ANDI, ANDI, and NDI controllers (**a**) Roll angular rate (**b**) Pitch angular rate (**c**) Yaw angular rate

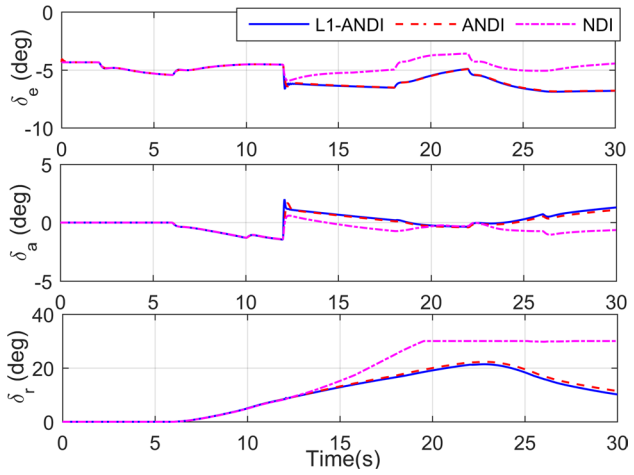

Fig. 12 Comparison results of control surface deflections

6 Conclusion

In this paper, a novel L1-ANDI control method is presented to reduce the model dependence of NDI control, and it is successfully applied to the design of the flight controller to improve the robustness of the aircraft against CG sudden shift, which may represent an important for the development of NDI control and to improve the flight quality and ensure the safe flight of an aircraft. The proposed L1-ANDI control method combines the merits of NDI control and L1 adaptive control, which is capable of weakening the influence of uncertain disturbances and decoupling the robustness and fast adaptation. Moreover, in the presence of uncertain disturbances, this method not only ensures steady-state performance but also takes the transient performance of a system into account.

Additionally, this paper establishes the nonlinear aircraft model with CG variations and designs the flight control law based on the proposed L1-ANDI approach. A series of simulation results are consistent with the theoretical analysis, demonstrating the robustness and effectiveness of this method.

Future work will focus on two aspects. On the one hand, the control performance and robustness of the designed LI-ANDI flight controller will be further verified in worse faults situations, such as surface damage and actuator stuck faults.

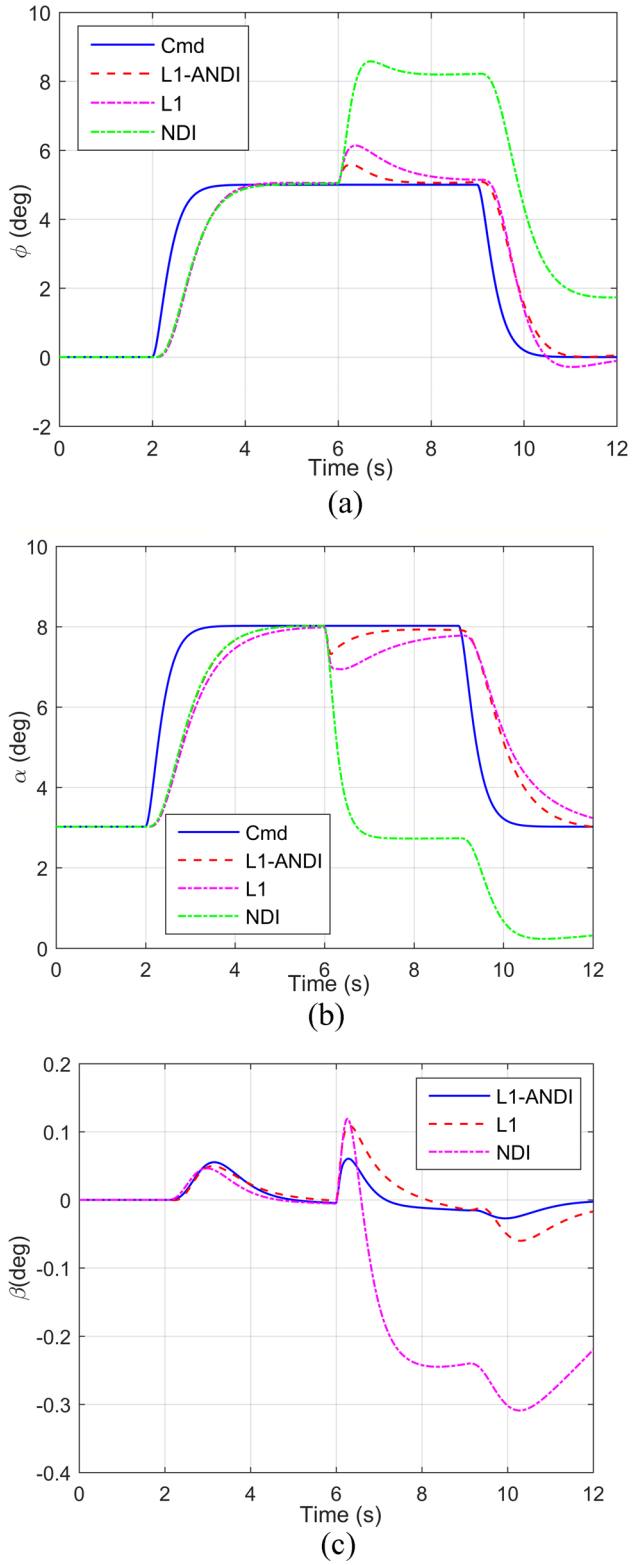

Fig. 13 Comparison results of attitude angle (**a**) Roll angle (**b**) Angle of attack (**c**) Sideslip angle

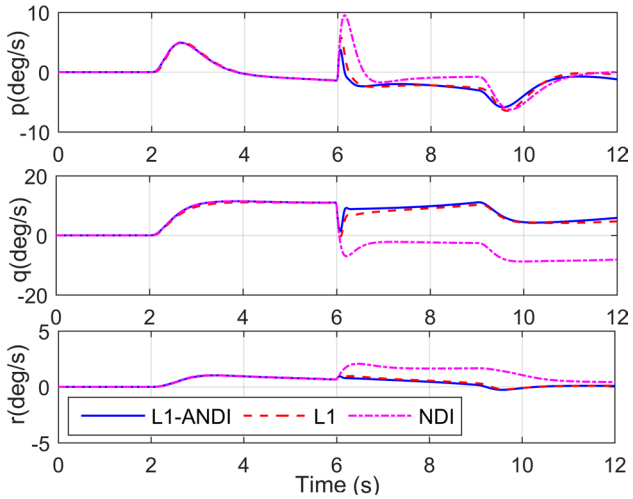

Fig. 14 Comparison results of angular rate

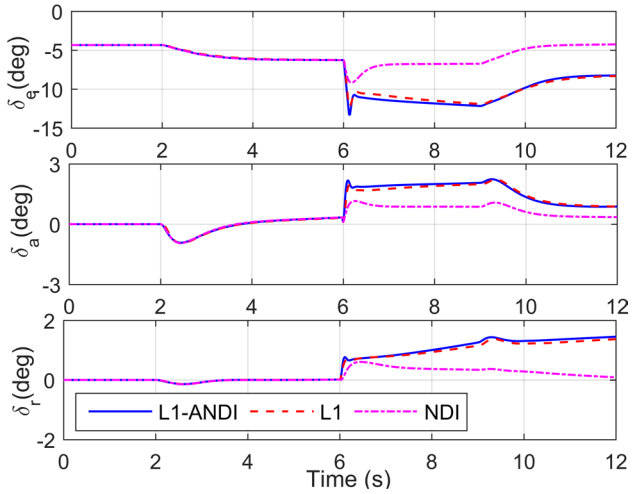

Fig. 15 Comparison results of control surface deflections (L1-ANDI, L1, and NDI denote attitude angle controllers with angular rate controllers based on L1-ANDI, L1 and NDI as inner loops, respectively)

On the other hand, the L1 adaptive structure-based nonlinear generalized dynamic inversion control will be further studied when the system that the number of control input is greater than that of the controlled states.

Acknowledgements The authors would like to express their gratitude to the Shaanxi Province Key Laboratory of Flight Control and Simulation Technology for supporting this research.

Funding This research work is funded by the National Natural Science Foundation of China (No. 62073266) and the Aeronautical Science Foundation of China (No. 201905053003).

Code availability Data sharing is not applicable to this article as no new data were created or analyzed in this study.

Declarations

Conflicts of interest interests The authors declared no potential conflicts of interest with respect to the research, authorship, and/or publication of this article.

Ethics approval Not applicable.

Consent to participate Not applicable.

Consent for publication All the authors agreed to publish this manuscript in the "Journal of Intelligent & Robotic Systems".

References

1. Smith, P.R., Patel, Y.: Translational motion control of VSTOL aircraft using nonlinear dynamic inversion, in: 20th Atmos. Flight Mech. Conf., 238–252 (1995). https://doi.org/10.2514/6.1995-3452
2. Lim, S., Kim, B.S.: Aircraft CAS design with input saturation using dynamic model inversion. Int. J. Control. Autom. Syst. **1**, 315–320 (2003)
3. Bin Hsiao, F., Duan, L.L., Lu, W.C.: Evaluation of nonlinear dynamic inversion technique applied to flight-path control. J. Chinese Soc. Mech. Eng. Trans. Chinese Inst. Eng. Ser. C/Chung-Kuo Chi Hsueh K. Ch'eng Hsuebo Pao. **29**, 171–177 (2008). https://doi.org/10.29979/JCSME.200804.0009
4. Snell, S.A., Enns, D.F., Garrard, W.L.: Nonlinear inversion flight control for a supermaneuverable aircraft. J. Guid. Control. Dyn. **15**, 976–984 (1992). https://doi.org/10.2514/3.20932
5. Wu, G., Meng, X., Wang, F.: Improved nonlinear dynamic inversion control for a flexible air-breathing hypersonic vehicle. Aerosp. Sci. Technol. **78**, 734–743 (2018). https://doi.org/10.1016/j.ast.2018.04.036
6. Sieberling, S., Chu, Q.P., Mulder, J.A.: Robust flight control using incremental nonlinear dynamic inversion and angular acceleration prediction. J. Guid. Control. Dyn. **33**, 1732–1742 (2010). https://doi.org/10.2514/1.49978
7. Wang, X., Van Kampen, E., Chu, Q.P., De Breuker, R.: Flexible aircraft gust load alleviation with incremental nonlinear dynamic inversion. J. Guid. Control. Dyn. **42**, 1519–1536 (2019). https://doi.org/10.2514/1.G003980
8. Mehedi, I.M., Shah, M.H.M.: Position Control of rotary flexible joint system using Adaptive dynamic inversion. IEEJ Trans. Electr. Electron. Eng. **17**, 96–102 (2022). https://doi.org/10.1002/tee.23491
9. He, Q., Tan, Y., Liu, X., Jia, Q., Liu, J.: Reconfigurable nonlinear dynamic inversion for attitude Control of a structurally damaged aircraft. IEEE Access. **8**, 199931–199943 (2020). https://doi.org/10.1109/ACCESS.2020.3035436
10. Wang, L., Zhang, Z., Zhu, Q., Wen, Z.: Longitudinal automatic carrier-landing control law rejecting disturbances and coupling based on adaptive dynamic inversion. Bull. Polish Acad. Sci. Tech. Sci. **69** (2021). https://doi.org/10.24425/bpasts.2020.136217
11. Joshi, G., Padhi, R.: Robust satellite formation flying using Dynamic Inversion with modified state observer. in: Proc. IEEE Int. Conf. Control Appl., 568–573 (2013). https://doi.org/10.1109/CCA.2013.6662810
12. Cao, C., Hovakimyan, N.: Design and analysis of a novel $\mathscr{L}1$ adaptive controller, part I: Control signal and asymptotic stability, in. Proc. Am. Control Conf., 3397–3402 (2006). https://doi.org/10.1109/acc.2006.1657243

13. Yu, L., Xiaoxiong, L., Hui, Z., Yueheng, Q.: Design of control law for Carrier-based Aircraft based on Ll adaptive control, in: 2018 IEEE CSAA Guid. Navig. Control Conf. CGNCC. **2018**, 2018. https://doi.org/10.1109/GNCC42960.2018.9019179
14. Xiaoxiong, L., Li, Y., Yuan, M.Q., Jian, S.: Gust alleviation controller for elastic aircraft based on L1 adaptive control, in: Proc. - 2017 Chinese Autom. Congr. CAC. **2017**(2017), 5382–5385. https://doi.org/10.1109/CAC.2017.8243737
15. Zhou, Y., Liu, H., Guo, H., Duan, X.: L1 adaptive dynamic inversion attitude control for unmanned aerial vehicle with actuator failures. Proc. Inst. Mech. Eng. Part G J. Aerosp. Eng. **233**, 4129–4140 (2019). https://doi.org/10.1177/0954410018814602
16. Campbell, S.F., Kaneshige, J.T.: A nonlinear dynamic inversion L1 adaptive controller for a Generic Transport Model. in: Proc. 2010 Am. Control Conf. ACC. **2010**, 862–867 (2010). https://doi.org/10.1109/acc.2010.5530704
17. Zuo, Z., Ru, P.: Augmented script L1 adaptive tracking control of quad-rotor unmanned aircrafts. IEEE Trans. Aerosp. Electron. Syst. **50**, 3090–3101 (2014). https://doi.org/10.1109/TAES.2014.120705
18. Song, H.T., Zhang, T., Zhang, G.L.: L1 adaptive state feedback controller for three-dimensional integrated guidance and control of interceptor. Proc. Inst. Mech. Eng. Part G J. Aerosp. Eng. **228**, 1693–1701 (2014). https://doi.org/10.1177/0954410013506332
19. Chang, J., Zhu, J., Liu, R., Dong, W.: Lateral Control for ultra-low altitude airdrop based on the L1 Adaptive Control augmentation. Int. J. Control. Autom. Syst. **16**, 461–477 (2018). https://doi.org/10.1007/s12555-017-0014-5
20. Luo, J., Cao, C.: Consensus in multi-agent systems with nonlinear uncertainties under a fixed undirected graph. Int. J. Control. Autom. Syst. **12**, 231–240 (2014). https://doi.org/10.1007/s12555-013-0220-8
21. Geiser, M., Xargay, E., Hovakimyan, N., Bierling, T., Holzapfel, F.: L1 adaptive augmented dynamic inversion controller for a high agility UAV. in: AIAA Guid. Navig. Control Conf., 2011 (2011). https://doi.org/10.2514/6.2011-6457
22. Van Heusden, K., Talebian, K., Dumont, G.A.: Analysis of L 1 adaptive state feedback control. Why does it approximate an implementable LTI controller? Eur. J. Control. **23**, 1–7 (2015). https://doi.org/10.1016/j.ejcon.2015.02.003
23. Maalouf, D., Chemori, A., Creuze, V.: L1 Adaptive depth and pitch control of an underwater vehicle with real-time experiments. Ocean Eng. **98**, 66–77 (2015). https://doi.org/10.1016/j.oceaneng.2015.02.002
24. Lee, H., Snyder, S., Hovakimyan, N.: L1 Adaptive output feedback augmentation for missile systems. IEEE Trans. Aerosp. Electron. Syst. **54**, 680–692 (2018). https://doi.org/10.1109/TAES.2017.2764218
25. Leman, T., Xargay, E., Dullerud, G., Hovakimyan, N., Wendel, T.: $\mathscr{L}1$ adaptive control augmentation system for the X-48B aircraft. AIAA Guid. Navig. Control Conf. Exhib. (2009). https://doi.org/10.2514/6.2009-5619
26. Hameduddin, I., Bajodah, A.H.: Nonlinear generalised dynamic inversion for aircraft manoeuvring control. Int. J. Control. **85**, 437–450 (2012). https://doi.org/10.1080/00207179.2012.656143
27. Ansari, U., Bajodah, A.H.: Hybrid direct-indirect Adaptive generalized dynamic inversion based attitude Control of autonomous underwater vehicles, in: 2018 IEEE Conf. Control Technol. Appl. CCTA. **2018**, 101–106 (2018). https://doi.org/10.1109/CCTA.2018.8511496
28. Hovakimyan, N., Cao, C.: L1 Adaptive Control Theory: Guaranteed Robustness with Fast Adaptation. [Bookshelf], IEEE Control. Syst. **31**(2011), 112–114 (2010). https://doi.org/10.1109/mcs.2011.941837
29. Praly, L.: Adaptive nonlinear regulation: estimation from the Lyapunov equation. IEEE Trans. Automat. Contr. **37**, 729–740 (1992). https://doi.org/10.1109/9.256328
30. Bacon, B.J., Gregory, I.M.: General equations of motion for a damaged asymmetric aircraft. in: AIAA Atmos. Flight Mech. Conf., 63–75 (2007). https://doi.org/10.2514/6.2007-6306
31. Hovakimyan, N., Lavretsky, E., Cao, C.: Adaptive dynamic inversion via time-scale separation. IEEE Trans. Neural Netw. **19**, 1702–1711 (2008). https://doi.org/10.1109/TNN.2008.2001221

Yu Li received his B.S. and M.S. from the Department of Automation, Northwestern Polytechnical University, Xi'an, China, in 2016 and 2019, respectively, where he is currently pursuing his Ph.D. in Control Science and Engineering. His research interests include flight control , adaptive control, and nonlinear dynamic inversion control.

Xiaoxiong Liu received a degree in Navigation, Guidance, and Control from the School of Automatics, Northwestern Polytechnical University, Xi'an, China, in 2006. He is currently an Associate Professor with the School of Automatics, Northwestern, Polytechnical University. His research interests include UAV navigation, fault diagnosis, and nonlinear flight control.

Qizhi He was born in September 1992. He received the B.Eng. degree from Northwestern Polytechnical University in 2013, and the MA.Sc. degree with distinction in the University of Leicester in 2015. He is currently pursuing the Ph.D. degree in control science and engineering in Northwestern Polytechnical University. He published more than ten articles in relevant fields. His research interest includes fault tolerant flight control and multi-sensor information fusion theory

Ruichen Ming received his B.S. and M.S. from the School of Automatics, Northwestern Polytechnical University, Xi'an, China, in 2017 and 2020, respectively, where he is currently pursuing his Ph.D. in Control Science and Engineering. His research interests include flight control , adaptive control, and nonlinear control.

Wei Huang received M.S. from the School of Automatics, Northwestern Polytechnical University, Xi'an, China, in 2019, respectively, where he is currently pursuing his Ph.D. in Control Science and Engineering. His research interests include flight control, state estimation, fault diagnosis, and reconfigurable control.

Weiguo Zhang is currently a professor with the School of Automatics, Northwestern Polytechnical University. China. He was a visiting researcher at the University of Salford, Salford, U.K. from 1988 to 1991. His research interests include navigation, guidance and control, intelligent flight control, and fault-tolerant control.